JACS
JOURNAL OF THE AMERICAN CHEMICAL SOCIETY
Article
pubs.acs.org/JACS

Differentiation of CC vs CXC Chemokine Dimers with GAG Octasaccharide Binding Partners: An Ion Mobility Mass Spectrometry Approach

Youjin Seo,[†] Armann Andaya,[†] Christian Bleiholder,[‡] and Julie A. Leary*[,†]

[†]Departments of Chemistry and Molecular and Cellular Biology, University of California, Davis, California 95616, United States
[‡]Department of Chemistry and Biochemistry, University of California, Santa Barbara, California 93106, United States

Supporting Information

ABSTRACT: Chemokines, 8 kDa proteins implicated in leukocyte migration via oligomerization, bind to glycosaminoglycans (GAGs) during the inflammation response as a means to regulate chemokine migration. Structural characterization of chemokines non-covalently bound to GAGs provides physiologically meaningful data in regard to routine inmmunosurveillance and disease response. In order to analyze the structures resulting from the GAG:chemokine interaction, we employed ion mobility mass spectrometry (IMMS) to analyze monocyte chemoattractant protein-1 (MCP-1), a CC chemokine, and interleukin-8 (IL-8), a CXC chemokine, along with their individual interactions with GAG heparin octasaccharides. We show that MCP-1 and IL-8 are physiologically present as a dimer, with MCP-1 having two variants of its dimeric form and IL-8 having only one. We also show that the MCP-1 dimer adopts two conformations, one extended and one compact, when bound to a dodecasulfated heparin octasaccharide. Binding of MCP-1 to heparin octasaccharide isomers of varying sulfation patterns results in similar arrival time distribution values, which suggests minimal distinguishing features among the resultant complexes. Additionally, tandem mass spectrometry (MS/MS) showed that the binding of MCP-1 to a heparin octasaccharide has different dissociation patterns when compared with the corresponding IL-8 bound dimer. Overall, IMMS and MS/MS were used to better define the structural tendencies and differences associated with CC and CXC dimers when associated with GAG octasaccharides.

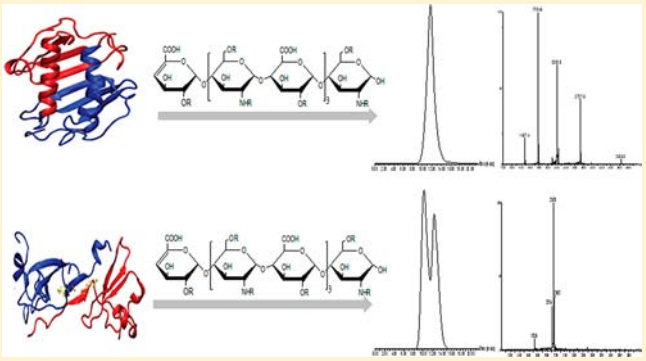

INTRODUCTION

Structural characterization of protein−carbohydrate interactions helps to advance the overall understanding of how these biomolecular complexes function physiologically during inflammation, cell growth, cell adhesion, and immune defense.[1−3] Investigations into the structural aspects of protein−carbohydrate interactions will likely lead to a better design of targeted therapies for diseases implicated when carbohydrates bind to proteins.[4−7] In addition, conformational changes resulting from the interactions between proteins and carbohydrates are important for understanding biological functionality within the cellular matrix.

To assess protein−carbohydrate complexes, standard methods have relied on analytical techniques such as FTIR, NMR, X-ray crystallography, and surface plasmon resonance imaging.[8−11] Despite their widespread use, these classic structural analysis methodologies are significantly challenged when investigating protein−carbohydrate complexes due to the need for large sample quantities, long analysis times, and carbohydrate heterogeneity. Currently, ion mobility mass spectrometry (IMMS) is emerging as a highly sensitive analytical technique capable of characterizing biomolecular complexes.[12−18] IMMS has successfully been used to structurally characterize small molecules, proteins, and their complexes on the basis of their arrival time distributions (ATDs) with subsequent calculation of collision cross sections (CCSs).[19−21] IMMS has been applied to the study of protein assemblies, structural stability, and distinct structural diversity of proteins and their complexes.[18−26] To this end, experimentally measured CCSs are comprehensively evaluated by comparison to theoretical CCS values as predicted for candidate structures (derived from X-ray, NMR, or modeling techniques) by computational algorithms. These include the projection approximation (PA),[27] exact hard-sphere scattering (EHSS),[28] trajectory,[29] and, more recently, projected superposition approximation (PSA) algorithms.[30−32]

Herein, we employ nano-electrospray ionization (nanoESI) coupled with quadrupole traveling wave ion mobility time-of-flight mass spectrometry (IM-TOF-MS) to analyze various conformations of chemokine−heparin complexes suspected of possessing different binding interfaces.

Received: November 9, 2012
Published: February 18, 2013

   dx.doi.org/10.1021/ja310915m | J. Am. Chem. Soc. 2013, 135, 4325−4332

Chemokine−heparin complexes have been shown to affect the cellular migration of leukocytes, which impacts the overall process of leukocyte activation—an essential step in the immune response pathway.[33,34] These 8−12 kDa proteins, consisting of 70−130 amino acids, maintain an equilibrium of 25% monomer and 75% oligomers (dimer, trimer, and/or tetramer) under normal physiological conditions. They have been implicated in autoimmune, respiratory, and other inflammatory immune responses. Chemokines, commonly classified into CC, CXC, C, or CXC3 according to their N-terminal sequence patterns, are highly basic proteins that inherently bind to negatively charged carbohydrates such as heparin, a member of the glycosaminoglycan (GAG) family of anionic polysaccharides.[35−37] Whether a chemokine is classified as CC or CXC appears to affect the dimer interface for the multimeric forms.[38] Heparin, a highly sulfated, linear, and heterogeneous polysaccharide, is found in the granules of mast cells and granulated cells.[1,39] The interaction between chemokines and heparin is responsible for *in vivo* and *in vitro* activity and is essential for regulating chemokine oligomerization, cell migration, and cellular recruitment.[38,40,41] Thus, it is important to determine if and/or how GAG binding affects the overall conformation of the complex.

Herein we investigate the structural features of monocyte chemoattractant protein-1 (MCP-1, CCL2) and interleukin-8 (IL-8, CXCL8), members of the CC and CXC chemokine families, respectively. Previous studies have used NMR spectroscopy, docking, and molecular dynamics (MD) to assess the conformations resulting from chemokine binding to GAG. The conformational differences between the two chemokines and those resulting from GAG binding are still ambiguous, while the essential residues for this binding have been identified for both MCP-1 and IL-8.[42−44] We use IMMS to specifically investigate the structural aspects of MCP-1 and IL-8 with and without heparin octasaccharides. Additionally, we vary both the degree and extent of sulfation on heparin octasaccharides and thus identify how these changes alter the chemokine−GAG assembly. Our results indicate that, under physiological conditions, both MCP-1 and IL-8 homodimerize; however, the CCSs reveal that the MCP-1 dimer adopts a more open or extended conformation than the IL-8 dimer. Additionally, when the MCP-1 dimer binds to dodecasulfated heparin octasaccharide, the resulting complex generates an even more compact conformation than the free dimer. This is in contrast to the ensuing structure of IL-8. Overall, our results suggest that fully sulfated GAGs cause a greater overall change in structure when binding to CC rather than CXC chemokines.

EXPERIMENTAL SECTION

Preparation of Chemokine, Heparin Octasaccharide, and Chemokine−Heparin Octasaccharide Complexes. Heparin octasaccharide was purchased from V-labs, Inc. (Covington, LA). Interleukin-8 was purchased from Abcam (San Francisco, CA). Myoglobin was purchased from Sigma-Aldrich Corp. (St, Louis, MO). The IonPac AS7 anion-exchange column was purchased from Dionex (Sunnyvale, CA). All solvents were of HPLC grade and purchased from Sigma-Aldrich Corp.

Monocyte chemokine attractant-1 (MCP-1) was expressed, isolated, and purified as described previously.[15] A 400 μM concentration of the chemokine was buffer-exchanged into 100 mM ammonium acetate (NH_4OAc), pH 6.8, using Bio-Gel P-6 (Bio-Rad, Hercules, CA). Heparin octasaccharide libraries with different sulfation patterns were prepared by chemical reactions as previously described (see Figure 1, below).[45] Briefly, the dodecasulfated heparin octasaccharide library was applied to a Dowex 50W (X-8, H+, 20−50 mesh) spin column with pyridine to obtain pyridinium salt forms. To prepare the N-desulfated heparin octasaccharide library, the pyridinium heparin octasaccharide library was reacted with dimethyl sulfoxide/water (95:5 v/v) at 50 °C for 24 h. To prepare the 6,O-desulfated heparin octasaccharide library, the pyridinium heparin octasaccharide library was reacted with *N*-methylpyrrolidinone/water (90:10 v/v) at 90 °C for 3 h, and then trimethylamine/sulfur trioxide (SO_3) and sodium carbonate were added. To prepare the 2,O-desulfated heparin octasaccharide library, the dodecasulfated heparin octasaccharide library was dissolved in 0.2 M NaOH, frozen, and lyophilized. The lyophilized powder was dissolved in water and adjusted to pH 7 with 10% acetic acid. All heparin octasaccharide libraries were separated by strong anion-exchange chromatography through the IonPac AS7 column (4.00 × 250 mm) with a linear gradient elution in order to obtain the desired species. The fractions were desalted using a 1 kDa molecular weight cutoff Dispo-Biodialyzer (The Nest Group Inc., Southborough, MA). Concentrations of purified chemokines and heparin octasaccharides were determined by nanoUV spectrophotometry at 232 and 280 nm, respectively (Thermo Fisher Scientific, Wilmington, DE). Chemokine−heparin octasaccharide complexes were prepared at a 1:1 concentration ratio of chemokine to heparin in 100 mM NH_4OAc, pH 6.8.

Ion Mobility Mass Spectrometry and Calibration Curve Calculations for Collision Cross Section Measurements. IMMS analysis was performed on the SYNAPT G2 HDMS system (Waters Corp., Milford, MA) with nanoESI. The G2 parameters were set as follows to allow optimal maintenance of the native conformations: capillary voltage, 0.8−0.9 kV; sample and extraction cone voltages, 5 and 1 V, respectively; trap and transfer collision energies, 5.0 and 0.0 V, respectively. Additional parameters: trap direct current (dc) bias, 35 V; trap cell gas (Ar) flow, 2.5 mL/min; and IM cell gas (N_2) flow, 90 mL/min. For optimal ion separation, the traveling wave velocity and pulse height were set at 108 m/s and 10.3 V, respectively, and the helium cell flow set was to 180 mL/min. To obtain the CCSs of chemokines and chemokine−heparin octasaccharide complexes, a calibration curve was constructed using myoglobin at a concentration of 0.1 mg/mL in MeOH/H_2O (1:1 v/v) with 1% formic acid. CCS calculations were performed using the absolute CCS of myoglobin obtained at the various charge states as previously described.[46−48] The CCS was determined by the formula derived from the calibration curve using a power fit equation and then corrected for charge state and reduced mass:

$$Y = 870.42X^{0.1097} \quad \text{where } R^2 = 0.99$$

where Y is the corrected CCS and X is the corrected arrival time of myoglobin.

To compare with experimental CCS measurements of chemokines, theoretical CCSs were estimated from PA and EHSS methods in a modified version of the MOBCAL program.[28,29] Additional comparisons were made with a newer theoretical calculation algorithm, PSA.[30−32] PDB files 1DOM and 1IL8 for MPC-1 dimer and IL-8 dimer, respectively, were obtained from the RCSB Protein Data Bank.[49]

Molecular Dynamics Calculations. MD calculations were performed using the Amber03 force field[50,51] starting from NMR structures deposited in the PDB (entries 1DOM and 1IL8). The SHAKE algorithm[52] was applied to constrain all bonds connecting hydrogen atoms, and the simulation time step was set to 2 ps. The temperature was kept at 300 K by Langevin dynamics with a collision frequency of 1 ps^{-1}.

Projected Superposition Approximation. The PSA model[30−32] computes molecular CCSs $\sigma_{PSA}(T)$ as a PA modified for the collective size and shape effects. These collective effects are accounted for in the PSA model by a superposition of atomic collision probabilities, $p_j(T,x)$, on a plane perpendicular to the axis of projection and a shape factor $\rho(T)$, respectively:

$$\Omega^{(1,1)}(T) \equiv \sigma_{\mathrm{PSA}}(T) = \rho(T)\langle\Omega_{\mathrm{PSA}}(T)\rangle = \rho(T)\frac{1}{n}\sum_{i=1}^{n}\tilde{\Omega}_i\left[\sum_{j=1}^{m}p_j(T,x)\right] \quad (1)$$

Both the atomic collision probabilities and the shape factor are, in general, temperature dependent. The shape factor, $\rho(T)$, for a specific molecule is evaluated using the relationship

$$\rho = A_{\mathrm{mol}}/A_{\mathrm{ce}} \quad (2)$$

where the areas for the molecular surface A_{mol} and the convex envelope A_{ce} are evaluated numerically for the molecule of interest. To this end, the molecular surface[53] is first generated numerically by alpha shape theory.[54−56] The resulting molecular surface is a triangulated mesh, which is then reduced in complexity by an edge-collapse algorithm[57] that reduces the number of vertices and edges of the molecular surface to a set fraction of the original mesh. The reduced triangulated mesh is then used to compute the convex envelope by the QuickHull algorithm.[58] The value of the molecular surface area A_{mol} is then corrected for those patches on the surface that are invisible to the buffer gas (see ref 30 for the numerical details). The rationale for this correction is that hidden parts of the molecular surface do not undergo collisions with the buffer gas and thus effectively do not contribute to the CCS. The atomic collision probability $p_j(T,x)$ for a hit between a randomly chosen point at position x on the plane perpendicular to the projection axis with an analyte atom placed at position R_j was defined[30] as

$$p_j(T,x) = \begin{cases} 1, & x \le q_{j,\mathrm{coll}}(T;r_{\mathrm{LJ}},\varepsilon_{\mathrm{LJ}}) \\ \alpha\, e^{-(x-q_{j,\mathrm{coll}})k_1T^{l_1}} + & \\ \quad (\alpha-1)\, e^{-(x-q_{j,\mathrm{coll}})k_2T^{l_2}}, & x > q_{j,\mathrm{coll}}(T;r_{\mathrm{LJ}},\varepsilon_{\mathrm{LJ}}) \end{cases} \quad (3)$$

The functional form of $p_j(T,x)$ accounts for the fact that the probability of a hit between the analyte and the buffer gas decreases with increasing temperature T and distance $x = |x - R_j|$ of point x from the atomic center R_j. The parameters r_{LJ} and $\varepsilon_{\mathrm{LJ}}$ define the atom−atom collision integrals $q_{j,\mathrm{coll}}$.[59] Any point that satisfies $x = |x - R_j| < q_{j,\mathrm{coll}}$ is considered a collision. Points with $x > q_{j,\mathrm{coll}}$ are no longer considered a sure collision. Instead, the PSA model assumes that the probability for a collision decays exponentially with increasing distance x, defined by the parameters α, k_1, k_2, l_1, and l_2. In general, the collision probability for $x > q_{j,\mathrm{coll}}$ depends on the temperature T of the measurements (see eq 3). Atomic collision probabilities can be different for each element; consequently, seven parameters, r_{LJ}, $\varepsilon_{\mathrm{LJ}}$, α, k_1, k_2, l_1, and l_2, were recently fitted for different elements based on experimental cross sections for several small organic and inorganic compounds.[31] PSA calculations carried out in this work are based on this parameter set.

RESULTS AND DISCUSSION

Mass Spectrometry and Ion Mobility Mass Spectrometry Analysis of MCP-1 and MCP-1 Dodecasulfated Heparin Octasaccharide Complexes. MCP-1 was subjected to nanoESI-quadrupole-IM-TOF-MS and was observed as both a monomer with 4+, 5+, and 6+ charge state distributions and a dimer with 9+ and 8+ charge state distributions (Figure 1). The presence of both monomer and dimer mirrors what is observed under physiological conditions.[38] Mass spectrometric analysis of MCP-1 bound to dodecasulfated heparin octasaccharide ($[DP8(SO_3)_{12}]$) revealed one $[DP8(SO_3)_{12}]$ bound to the MCP-1 dimer ($(MCP\text{-}1)_2$) at the 8+ and 9+ charge states. Observation of $[DP8(SO_3)_{12}]$ with preferential binding to a dimer and not a monomer further validates MCP-1 oligomerization as a necessary step to induce MCP-1 activity.[40] When compared to heparin free dimer, the $(MCP\text{-}1)_2$:

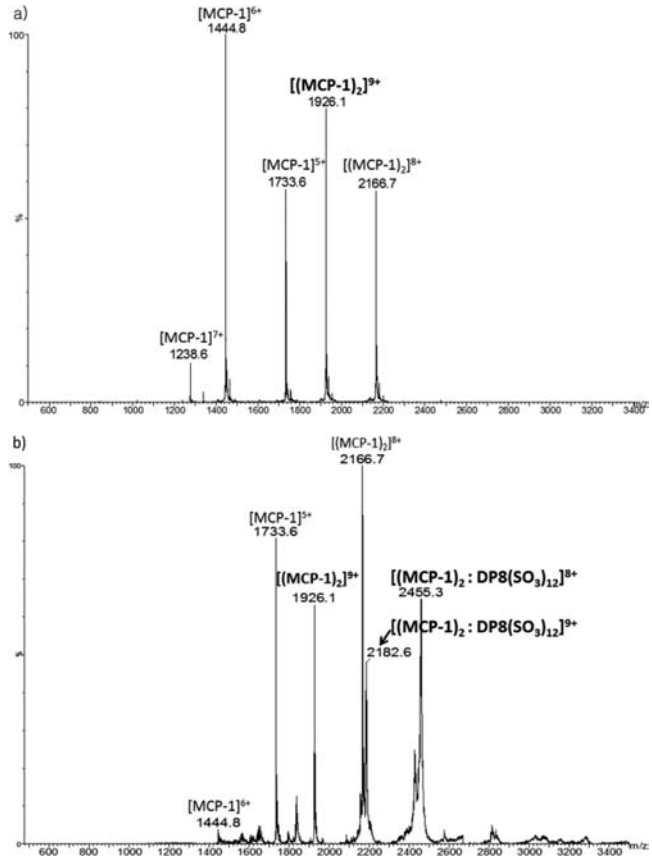

Figure 1. Mass spectra of (a) 20 μM MCP-1 and (b) 20 μM MCP-1:$[DP8(SO_3)_{12}]$ complex dissolved in 100 mM NH_4OAc, pH 6.8. MCP-1 and $(MPC\text{-}1)_2$ denote the monomer and dimer forms, respectively. $[DP8(SO_3)_{12}]$ represents the dodecasulfated heparin octasaccharide shown in Figure 3.

$[DP8(SO_3)_{12}]$ complexes showed little difference in their charge state distributions. To further investigate the effect of $[DP8(SO_3)_{12}]$ binding on MCP-1's charge states, MCP-1 and its complexes were infused using nanoESI under negative ion detection. Both species exist as dimer complexes at the 7− charge state (Figure S1). Thus, the highly negative charges inherent in $[DP8(SO_3)_{12}]$ have a minimal impact on the overall charge of MCP-1−heparin octasaccharide complexes.

After observation of heparin's effect on the charge state of MCP-1, the conformation of MCP-1 and MCP-1:$[DP8(SO_3)_{12}]$ complexes was investigated using IMMS. The ATDs of free MCP-1 dimer and dimer bound to $[DP8(SO_3)_{12}]$ were measured. The ATDs of $(MCP\text{-}1)_2$ and $(MCP\text{-}1)_2$:$[DP8(SO_3)_{12}]$ were obtained for the 9+ charge state (Figure 2). Two arrival times for the free $(MCP\text{-}1)_2$ were observed, one at 9.76 ± 0.06 ms and a second, more predominant ion population at 12.1 ± 0.06 ms. The presence of two conformations for the $(MCP\text{-}1)_2$ may reflect its innate flexible N-terminal region, previously shown by structural studies as divergent dimer structures.[44] The arrival times of $(MCP\text{-}1)_2$:$[DP8(SO_3)_{12}]$ were 10.4 ± 0.06 and 12.2 ± 0.06 ms for the major and minor ion populations, respectively, and ion population areas for free and complexed MCP-1 were 39.3% and 61.3%, respectively (Table 1). The $(MCP\text{-}1)_2$:$[DP8(SO_3)_{12}]$ complex maintains its compact conformation, with an increase of 22% compared to that of $(MCP\text{-}1)_2$ alone (Figure 2). This observation suggests that the $[DP8(SO_3)_{12}]$ preferentially binds to a more compact

dx.doi.org/10.1021/ja310915m | J. Am. Chem. Soc. 2013, 135, 4325−4332

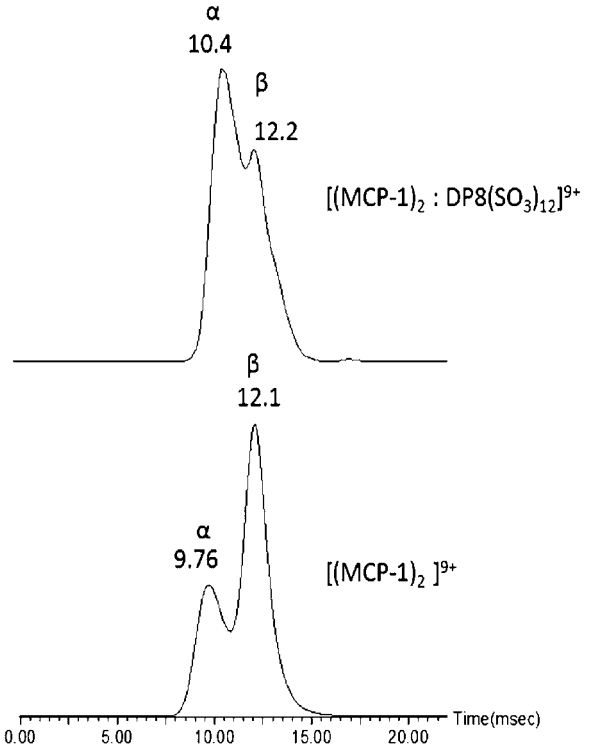

Figure 2. Arrival time distributions for $(MCP\text{-}1)_2$ and $[(MCP\text{-}1)_2{:}DP8(SO_3)_{12}]$ at the 9+ charge state. The arrival times are recorded in milliseconds. The arrival times were obtained from three individual measurements with a standard deviation of ±0.06 ms.

Table 1. Ion Population Area of $[(MCP\text{-}1)_2{:}DP8(SO_3)_{12}]$ at the 9+ Charge State in Ion Mobility Spectra[a]

	area (%)	
	α (compact conformation)	β (extended conformation)
$(MCP\text{-}1)_2$	39.29 ± 0.4	60.71 ± 0.5
$(MCP\text{-}1)_2{:}DP8(SO_3)_{12}$	61.33 ± 0.5	38.67 ± 0.5

[a]The data are from three individual measurements.

conformation of $(MCP\text{-}1)_2$, which results in an overall increase of the compact ion population. Our finding also suggests that $[DP8(SO_3)_{12}]$ may promote compact complex formation and/or constrain the inherent floppiness of the N-terminus where heparin normally binds.

Observation of the effects of $[DP8(SO_3)_{12}]$ binding to MCP-1 led us to examine the effects that differing sulfation patterns have on overall MCP-1–heparin octasaccharide complex conformation. In a previous study, we showed that different sulfation patterns on heparin octasaccharide isomers induce changes in their overall conformation, and these isomers could be individually separated and analyzed using IMMS analysis.[45] Despite the differences in ATDs observed for different heparin octasaccharide sulfation patterns, when bound to MCP-1, the ATDs of N-desulfated ([DP8(1)]), 2,O-desulfated ([DP8(2)]), and 6,O-desulfated ([DP8(3)]) octasaccharides (Figure 3) bound to the dimer showed little variance in both arrival times and ion population areas (Table S1, Figure S2). Selective sulfation removal from heparin octasaccharides seems to have minimal impact on overall conformation for the $(MCP\text{-}1)_2$–heparin octasaccharide complexes. Unlike $[DP8(SO_3)_{12}]$, the differently modified sulfated heparin octasaccharides did not favor the formation of the compact structure (Table S1, Figure S2). This observation demonstrates the specificity of the compact structure and its formation under conditions when MCP-1 is a dimer and heparin displays a high degree of sulfation. Previous research has reported that charge state distributions of proteins and protein complexes depend on the protein surface area in an ESI system.[60] The observation of similar CCSs of free $(MCP\text{-}1)_2$ and (MCP-1)–heparin octasaccharide complexes was shown to be consistent with the same charge state distribution.

We then measured CCSs for each of the two IM populations. The two CCSs for the 9+ charge state $(MCP\text{-}1)_2$ were 1811 and 1876 Å^2 (Table S1). These experimental CCSs were compared to the PA and EHSS theoretically derived values of 1770 and 2226 Å^2, respectively. The experimental values lie between the two models of theory as previously observed by us and other.[16,47] However, given that PA can significantly underestimate CCS measurements, we employed the accurate trajectory (TJM) and PSA method[30−32] as well and obtained theoretical values of 2087 (PSA) and 2245 Å^2 (TJM). Clearly these values are much larger than the experimental values and outside the previously calculated theoretical values obtained using PA and EHSS methods. Consequently, we performed short gas-phase MD calculations and were able to provide a refined model of the NMR structure (Figure 4). The new resulting theoretical CCSs were determined to be 1853 (TJM) and 1821 Å^2 (PSA), values now in very close agreement with the experimental CCS (Table S2). The refined MCP-1

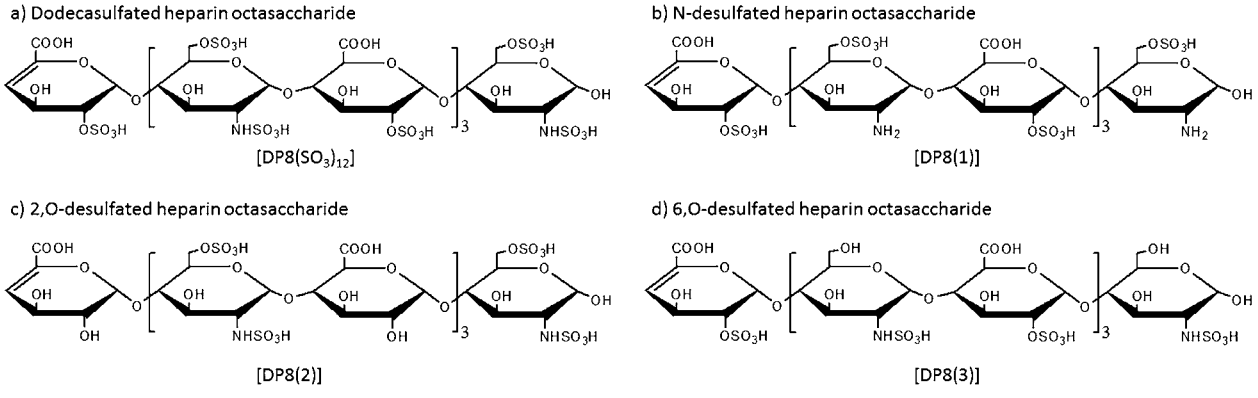

Figure 3. Heparin octasaccharide structures.

dx.doi.org/10.1021/ja310915m | J. Am. Chem. Soc. 2013, 135, 4325−4332

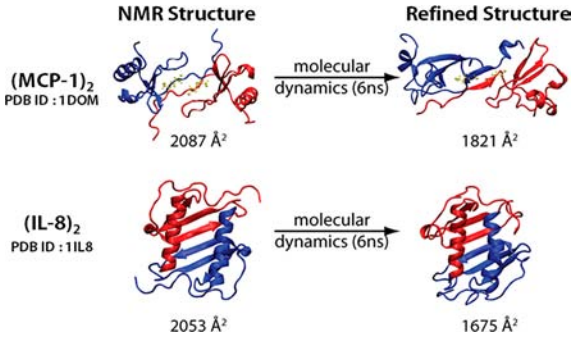

Figure 4. 3D structures and PSA collision cross sections for NMR and refined structures of $(MCP\text{-}1)_2$ (top) and $(IL\text{-}8)_2$ (bottom). The PDB files are from the RCSB PDB database.

structure retains the dimer topology of the NMR structure, which further corroborates that the MCP-1 dimer is stable within the gas phase. Furthermore, we note that IMMS is able to reveal the co-existence of two distinct conformations for $(MCP\text{-}1)_2$ in a steady state, an observation that traditional methods have thus far been unable to provide. The exact structure of the second $(MCP\text{-}1)_2$ with a CCS of 1876 Å^2 is currently under investigation and will be discussed in a forthcoming paper. The CCSs measured for $(MCP\text{-}1)_2$ bound to heparin octasaccharides of varying degree of sulfation showed negligible differences in their CCS of 1830−1880 Å^2, compared to the $(MCP\text{-}1)_2$ alone (Table S1).

Comparison between MCP-1 (CC Chemokine) and IL-8 (CXC Chemokine). Having characterized the protein−carbohydrate interaction between MCP-1 (a CC chemokine) and heparin octasaccharide GAGs, we next investigated this same interaction with IL-8 (a CXC chemokine). Structures obtained by X-ray and NMR analysis (Figure 4) show distinct differences between CC and CXC dimers; thus, we postulated that GAG binding also would likely exhibit unique differences between MCP-1 and IL-8. IL-8 belongs to the subfamily of CXC chemokines classified as $(ELR)^+$.[61,62] $(ELR)^+$ CXC chemokines are known to be fast responding chemokines to conditions of inflammation,[62] and thus, there is speculation whether a mechanism for this fast acting response may be deduced from certain structurally salient features ascertained from our analysis. Since GAG binding to MCP-1 results in physiological activity, we next bound IL-8 to GAG and compared and contrasted this interaction with that for MCP-1.

IMMS of IL-8 revealed a dimer in the 8+ and 9+ charge states and a monomer in the 4+, 5+, and 6+ charge states (Figure 5a). Similar to MCP-1, the existence of monomer and dimer is in agreement with that observed in solution.[42,63] As was the case with the MCP-1 dimer, [DP8(1)] bound to the dimeric form of IL-8 (Figure 5b and Figure S3).[37,64] The ATDs of $(IL\text{-}8)_2$ and $(IL\text{-}8)_2$:[DP8(1)] revealed CCSs of 1710 and 1860 Å, respectively. PSA cross sections computed for the refined NMR structures of $(IL\text{-}8)_2$ ($\sigma_{PSA}(T)$ = 1675 Å^2) are in close agreement with the experiment (Figure 4).[30] These observed CCSs for the CXC chemokine differed dramatically from that for the CC chemokine (Figure 6). IMMS results show that the prototype CXC dimer $(IL\text{-}8)_2$ takes on a more compact dimer fold than the archetype CC dimer $(MCP\text{-}1)_2$. Our observation thus is in agreement with previous structural studies showing the closer orientation of the two α-helices for $(IL\text{-}8)_2$ than that for $(MCP\text{-}1)_2$[63,65] (Figure 4).

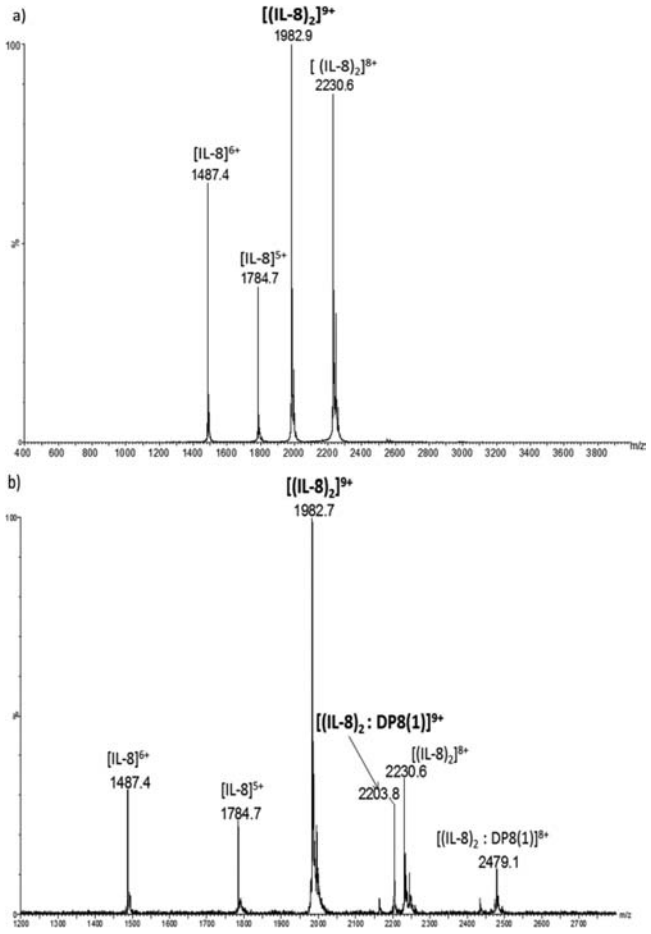

Figure 5. Mass spectra of (a) 20 μM IL-8 and (b) 20 μM IL-8:[DP8(1)] complexes dissolved in 100 mM NH_4OAc, pH 6.8. IL-8 and $(IL\text{-}8)_2$ denote a monomeric and a dimeric form, respectively. [DP8(1)] is represented as a N-desulfated heparin octasaccharide (see Figure 3 for structure).

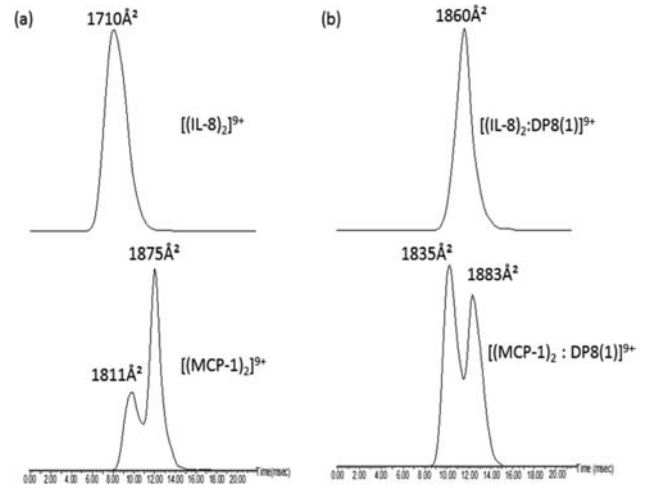

Figure 6. Arrival time distributions for (a) $(MCP\text{-}1)_2$ and $(IL\text{-}8)_2$ and (b) $[(MCP\text{-}1)_2$:DP8(1)] and/or $[(IL\text{-}8)_2$:DP8(1)] at the 9+ charge state. Collision cross sections were obtained from three individual measurements with a standard deviation of ±1.6 to ±2.5. [DP8(1)] is represented as a N-desulfated heparin octasaccharide.

As with $(IL\text{-}8)_2$, we observed a single conformation for the $(IL\text{-}8)_2$:[DP8(1)] complex with a CCS of 1860 Å^2. This is in

dx.doi.org/10.1021/ja310915m | J. Am. Chem. Soc. 2013, 135, 4325−4332

contrast to the two conformations observed for the $(MCP\text{-}1)_2$:[DP8(1)] complex. The innate flexibility of $(MCP\text{-}1)_2$'s N-terminus versus IL-8's rigidity may explain the single conformation observed for $(IL\text{-}8)_2$.[44,63] Regardless of the structural differences between $(MCP\text{-}1)_2$ and $(IL\text{-}8)_2$, we have shown the significant utility of resolving these conformational differences using IMMS. There is little structural information within the scientific literature regarding $(MCP\text{-}1)_2$–heparin complexes, and the data provided here constitute the first report showing different structural specificity for GAG binding to CC vs CXC chemokines.

Tandem Mass Spectrometry Analysis of MCP-1 Dimer–Heparin Octasaccharide Complexes. In order to further characterize the subpopulations observed for the $(MCP\text{-}1)_2$–heparin octasaccharide complexes, collision-induced dissociation (CID) was employed for the 9^+ precursor ions. Individual ion populations were separated in the IM cell with subsequent diagnostic fragment ions of each analyzed in the transfer cell. Isolated $(MCP\text{-}1)_2$ ions for both compact and extended conformations were completely dissociated into 3^+, 4^+, 5^+ and 6^+ monomers (Figure 7a). Tandem mass spectrometry (MS/MS) of the $(MCP\text{-}1)_2$:$[DP8(SO_3)_{12}]^{9+}$ (Figure 7b) and $(MCP\text{-}1)_2$:$[DP8(1)]^{9+}$ (Figure 8a) were performed under the same collision energy of 50 V for both the extended and compact conformations for each of the two complexes. Loss of SO_3 appears prevalent only for extended conformations and is nonexistent for the compact structure.

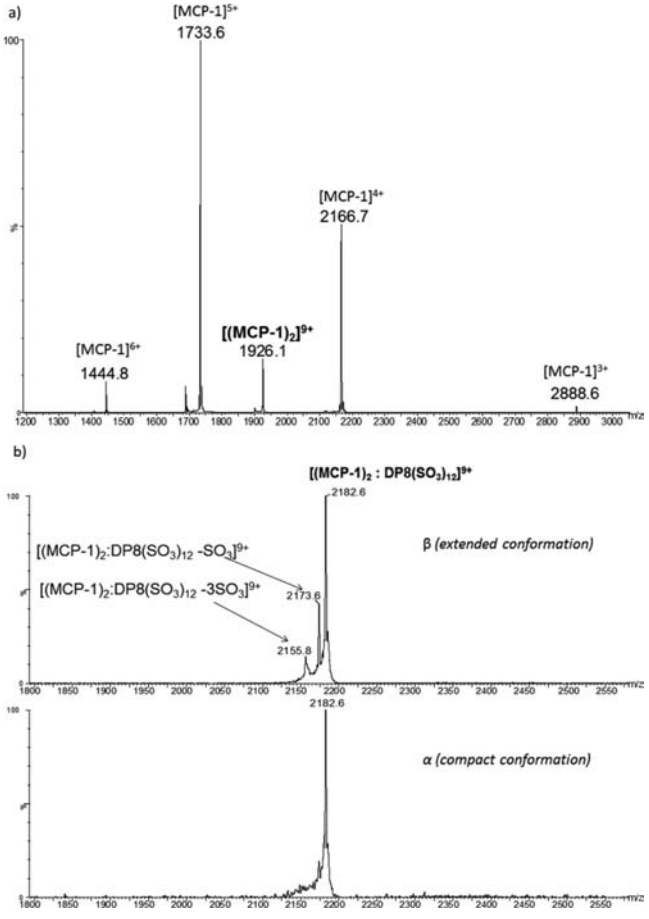

Figure 7. MS/MS spectra of (a) 20 μM $[(MPC\text{-}1)_2]^{9+}$ and (b) 20 μM $[(MCP\text{-}1)_2$:$DP8(SO_3)_{12}]^{9+}$. The precursor ions are subject to 50 V collision energy in the transfer cell.

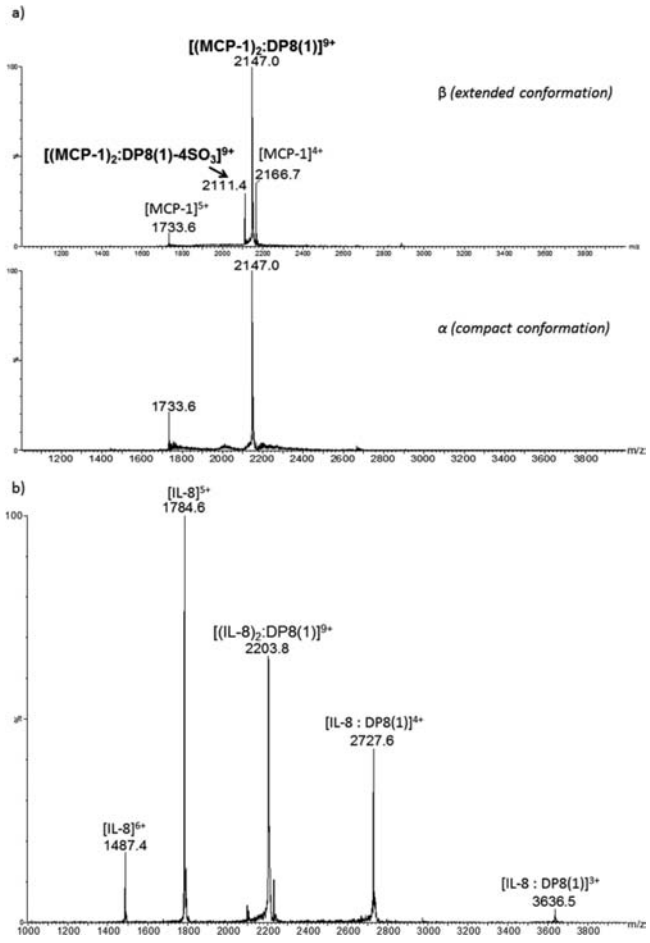

Figure 8. MS/MS spectra of (a) 20 μM $[(MCP\text{-}1)_2$:$DP8(1)]^{9+}$ and (b) $[(IL\text{-}8)_2$:$DP8(1)]^{9+}$. The precursor ion is subject to 50 V collision energy in the transfer cell.

$[DP8(SO_3)_{12}]$ additionally prevents the dissociation of the $(MCP\text{-}1)_2$ into its monomeric form which is in contrast to that observed with [DP8(1)] binding (Figures 7b and 8a). This suggests that $[DP8(SO_3)_{12}]$ binds with tight affinity to one of the $(MCP\text{-}1)_2$ isoforms yielding a very stable compact conformation that both maintains the $(MCP\text{-}1)_2$ and protects against SO_3 loss within the transfer cell. For either the extended or compact conformation, the binding of $[DP8(SO_3)_{12}]$ to the $(MCP\text{-}1)_2$ protects the $(MCP\text{-}1)_2$ from dissociating into its monomeric subunits thus maintaining the biologically active dimer. In addition to $[DP8(SO_3)_{12}]$ and [DP8(1)], we investigated two other modified heparin octasaccharides and their interaction with MCP-1. The 2,O-desulfated ([DP8(2)]) and 6,O-desulfated ([DP8(3)]) species were each non-covalently bound to $(MCP\text{-}1)_2$ followed by CID analysis. The data demonstrate that the fragmentation patterns were similar to that of $(MCP\text{-}1)_2$:[DP8(1)] and independent of sulfation pattern (Figure S4). Collectively, these results highlight the importance of sulfation in maintaining the GAG–chemokine structure, as only the $[DP8(SO_3)_{12}]$ preserves its structure under CID. Our analysis illustrates that the location of sulfates on the GAG does not adversely influence the GAG–chemokine structure; rather, the absence of sulfation proves detrimental to maintaining the integrity of the complex.

dx.doi.org/10.1021/ja310915m | J. Am. Chem. Soc. 2013, 135, 4325–4332

We next collisionally activated $(IL\text{-}8)_2$ and $(IL\text{-}8)_2$:[DP8(1)]. Isolated $[(IL\text{-}8)_2]^{9+}$ was completely dissociated into 3+, 4+, 5+, and 6+ monomers (Figure S5). MS/MS of the $(IL\text{-}8)_2$:[DP8(1)] ion in the 9+ charge state resulted in a IL-8 monomer (IL-8) in the 5+ and 6+ charge states, and (IL-8):[DP8(1)] in the 3+ and 4+ charge states (Figure 8b). Clearly, $(IL\text{-}8)_2$:[DP8(1)] dissociates into its monomers with no SO_3 loss, whereas $(MCP\text{-}1)_2$:[DP8(1)] was retained at the expense of SO_3 removal thus highlighting the different affinity of GAG to CXC and CC chemokines. Regarding the binding interactions, previous reports have shown possible conformations of the chemokine−GAG complexes in which the GAG is positioned either parallel or perpendicular relative to the helical axis of the chemokine dimer.[43,64,66,67] Our analysis via MS/MS for $(IL\text{-}8)_2$:[DP8(1)] suggests that [DP8(1)] binds firmly and parallel to the outside of one of the $(IL\text{-}8)_2$ helices, resulting in production of (IL-8):[DP8(1)] and an IL-8 monomer during CID.

In contrast to $(IL\text{-}8)_2$, [DP8(1)] likely straddles $(MCP\text{-}1)_2$ in a horseshoe-like manner[64,68] at the dimer interface (Figure 8), thus preventing dissociation of the $(MCP\text{-}1)_2$ into its monomeric form. This horseshoe-like binding of [DP8(1)] to $(MCP\text{-}1)_2$ may be a unique feature of CC chemokines. Unlike the CC chemokine $(MCP\text{-}1)_2$, the CXC chemokine $(IL\text{-}8)_2$ presents as only one conformation with or without GAG binding. Thus, the observation of two conformations of $(MCP\text{-}1)_2$ and only one for the $(IL\text{-}8)_2$ suggests a more unique or rigid specificity for GAG binding in the case of the CXC chemokine. Additionally, dissociation of the CXC chemokine−GAG complex shows retention of the GAG on one of the monomers and no SO_3 loss. This is in contrast to the CC chemokine−GAG complex, which results in SO_3 loss from the GAG and subsequent production of a monomer.

The degree of GAG sulfation, its sulfation pattern, and its interaction to chemokine likely influence the overall biological activity of the chemokine−GAG complex.[69,70] Thus, under instances prior to inflammation, in a highly dynamic milieu of chemokines and their respective GAG binding partners, CXC chemokines may exist as monomers bound to appropriately sulfated GAGs and would become biologically active simply by binding to another CXC chemokine under inflammatory conditions.[71] However, CC chemokines may be bound to inappropriately sulfated GAGs and/or may exist as free monomers, thus necessitating multiple binding steps to attain physiological relevance under conditions of inflammation. These extra binding steps may be absent from CXC chemokines and thus present a novel hypothesis for the rapid response of the $(ELR)^+$ CXC chemokine IL-8 under instances of inflammation.[62]

CONCLUSION

We have characterized the structural interaction of MCP-1 ($(MCP\text{-}1)_2$) and IL-8 dimers ($(IL\text{-}8)_2$) with and without heparin octasaccharides using ion mobility mass spectrometric analysis and tandem mass spectrometry. We have shown that the CCSs of $(MCP\text{-}1)_2$ and $(IL\text{-}8)_2$ are in agreement with theoretical CCSs calculated from projected superposition approximation. Our studies demonstrate that $(MCP\text{-}1)_2$ adopts a more compact structure when bound to dodecasulfated heparin octasaccharides. With MS/MS analysis, we have shown that heparin octasaccharide prevents $(MCP\text{-}1)_2$ dissociation but not $(IL\text{-}8)_2$ dissociation. This latter finding further supports the notion of specific and different patterns for $(MCP\text{-}1)_2$ versus $(IL\text{-}8)_2$ binding to heparin octasaccharides. The conformational characterization of MCP-1 and IL-8−heparin octasaccharide complexes will likely also lead to a better understanding of their structure−function relationships.

ASSOCIATED CONTENT

Supporting Information

Additional mass spectra, MS/MS spectra, IM spectra, and CCS measurements of MCP-1, IL-8, and MCP-1−heparin octasaccharide complexes. This material is available free of charge via the Internet at http://pubs.acs.org.

AUTHOR INFORMATION

Corresponding Author

jaleary@ucdavis.edu

Notes

The authors declare no competing financial interest.

ACKNOWLEDGMENTS

We acknowledge National Institute of Health grant GM47356 to J.A.L. for supporting this research.

REFERENCES

(1) Varki, A. *Essentials of glycobiology*, 2nd ed.; Cold Spring Harbor Laboratory Press: Cold Spring Harbor, NY, 2009.
(2) Dwek, R. A. *Chem. Rev.* **1996**, *96*, 683.
(3) Lee, Y. C. *FASEB J.* **1992**, *6*, 3193.
(4) Qasba, P. K.; Ramakrishnan, B.; Boeggeman, E. *Curr. Drug Targets* **2008**, *9*, 292.
(5) Ernst, B.; Magnani, J. L. *Nat. Rev. Drug Discov.* **2009**, *8*, 661.
(6) Karlsson, K. A. *Trends Pharmacol. Sci.* **1991**, *12*, 265.
(7) Mazik, M. *Chem. Soc. Rev.* **2009**, *38*, 935.
(8) Weis, W. I.; Drickamer, K. *Annu. Rev. Biochem.* **1996**, *65*, 441.
(9) Poveda, A.; Jimenez-Barbero, J. *Chem. Soc. Rev.* **1998**, *27*, 133.
(10) Smith, E. A.; Thomas, W. D.; Kiessling, L. L.; Corn, R. M. *J. Am. Chem. Soc.* **2003**, *125*, 6140.
(11) de la Fuente, J. M.; Penades, S. *Glycoconjugate J.* **2004**, *21*, 149.
(12) Sinz, A. *ChemMedChem* **2007**, *2*, 425.
(13) Loo, J. A. *Mass Spectrom. Rev.* **1997**, *16*, 1.
(14) Leary, J. A.; Schenauer, M. R.; Stefanescu, R.; Andaya, A.; Ruotolo, B. T.; Robinson, C. V.; Thalassinos, K.; Scrivens, J. H.; Sokabe, M.; Hershey, J. W. *J. Am. Soc. Mass Spectrom.* **2009**, *20*, 1699.
(15) Schenauer, M. R.; Leary, J. A. *Int. J. Mass Spectrom.* **2009**, *287*, 70.
(16) Ninonuevo, M. R.; Leary, J. A. *Anal. Chem.* **2012**, *84*, 3208.
(17) Schenauer, M. R.; Meissen, J. K.; Seo, Y.; Ames, J. B.; Leary, J. A. *Anal. Chem.* **2009**, *81*, 10179.
(18) Bleiholder, C.; Dupuis, N. F.; Wyttenbach, T.; Bowers, M. T. *Nature Chem.* **2011**, *3*, 172.
(19) von Helden, G.; Wyttenbach, T.; Bowers, M. T. *Science* **1995**, *267*, 1483.
(20) Bohrer, B. C.; Mererbloom, S. I.; Koeniger, S. L.; Hilderbrand, A. E.; Clemmer, D. E. *Annu. Rev. Anal. Chem.* **2008**, *1*, 293.
(21) Akashi, S. *Med. Res. Rev.* **2006**, *26*, 339.
(22) Uetrecht, C.; Rose, R. J.; van Duijn, E.; Lorenzen, K.; Heck, A. J. R. *Chem. Soc. Rev.* **2010**, *39*, 1633.
(23) Pukala, T. L.; Ruotolo, B. T.; Zhou, M.; Politis, A.; Stefanescu, R.; Leary, J. A.; Robinson, C. V. *Structure* **2009**, *17*, 1235.
(24) Wang, S. C.; Politis, A.; Di Bartolo, N.; Bavro, V. N.; Tucker, S. J.; Booth, P. J.; Barrera, N. P.; Robinson, C. V. *J. Am. Chem. Soc.* **2010**, *132*, 15468.
(25) Uetrecht, C.; Barbu, I. M.; Shoemaker, G. K.; van Duijn, E.; Heck, A. J. R. *Nature Chem.* **2011**, *3*, 126.
(26) Bernstein, S. L.; Dupuis, N. F.; Lazo, N. D.; Wyttenbach, T.; Condron, M. M.; Bitan, G.; Teplow, D. B.; Shea, J. E.; Ruotolo, B. T.; Robinson, C. V.; Bowers, M. T. *Nature Chem.* **2009**, *1*, 326.

(27) Wyttenbach, T.; von Helden, G.; Batka, J. J.; Carlat, D.; Bowers, M. T. *J. Am. Soc. Mass Spectrom.* **1997**, *8*, 275.
(28) Shvartsburg, A. A.; Jarrold, M. F. *Chem. Phys. Lett.* **1996**, *261*, 86.
(29) Mesleh, M. F.; Hunter, J. M.; Shvartsburg, A. A.; Schatz, G. C.; Jarrold, M. F. *J. Phys. Chem.* **1996**, *100*, 16082.
(30) Bleiholder, C.; Wyttenbach, T.; Bowers, M. T. *Int. J. Mass Spectrom.* **2011**, *308*, 1.
(31) Bleiholder, C.; Contreras, S.; Do, T. D.; Bowers, M. T. *Int. J. Mass Spectrom.* **2012**, in press.
(32) Anderson, S. E.; Bleiholder, C.; Brocker, E. R.; Stang, P. J.; Bowers, M. T. *Int. J. Mass Spectrom.* **2012**, *330*, 78.
(33) Sallusto, F.; Baggiolini, M. *Nat. Immunol.* **2008**, *9*, 949.
(34) Webb, L. M.; Ehrengruber, M. U.; Clark-Lewis, I.; Baggiolini, M.; Rot, A. *Proc. Natl. Acad. Sci. U.S.A.* **1993**, *90*, 7158.
(35) Cyster, J. G. *Science* **1999**, *286*, 2098.
(36) Rossi, D.; Zlotnik, A. *Annu. Rev. Immunol.* **2000**, *18*, 217.
(37) Hoogewerf, A. J.; Kuschert, G. S. V.; Proudfoot, A. E. I.; Borlat, F.; ClarkLewis, I.; Power, C. A.; Wells, T. N. C. *Biochemistry* **1997**, *36*, 13570.
(38) Lau, E. K.; Paavola, C. D.; Johnson, Z.; Gaudry, J. P.; Geretti, E.; Borlat, F.; Kungl, A. J.; Proudfoot, A. E.; Handel, T. M. *J. Biol. Chem.* **2004**, *279*, 22294.
(39) Powell, A. K.; Yates, E. A.; Fernig, D. G.; Turnbull, J. E. *Glycobiology* **2004**, *14*, 17r.
(40) Proudfoot, A. E. I.; Handel, T. M.; Johnson, Z.; Lau, E. K.; LiWang, P.; Clark-Lewis, I.; Borlat, F.; Wells, T. N. C.; Kosco-Vilbois, M. H. *Proc. Natl. Acad. Sci. U.S.A.* **2003**, *100*, 1885.
(41) Hirose, J.; Kawashima, H.; Yoshie, O.; Tashiro, K.; Miyasaka, M. *J. Biol. Chem.* **2001**, *276*, 5228.
(42) Baldwin, E. T.; Weber, I. T.; Stcharles, R.; Xuan, J. C.; Appella, E.; Yamada, M.; Matsushima, K.; Edwards, B. F. P.; Clore, G. M.; Gronenborn, A. M.; Wlodawer, A. *Proc. Natl. Acad. Sci. U.S.A.* **1991**, *88*, 502.
(43) Bitomsky, W.; Wade, R. C. *J. Am. Chem. Soc.* **1999**, *121*, 3004.
(44) Lubkowski, J.; Bujacz, G.; Boque, L.; Domaille, P. J.; Handel, T. M.; Wlodawer, A. *Nat. Struct. Biol.* **1997**, *4*, 64.
(45) Seo, Y.; Andaya, A.; Leary, J. A. *Anal. Chem.* **2012**, *84*, 2416.
(46) Ruotolo, B. T.; Benesch, J. L.; Sandercock, A. M.; Hyung, S. J.; Robinson, C. V. *Nat. Protoc.* **2008**, *3*, 1139.
(47) Scarff, C. A.; Thalassinos, K.; Hilton, G. R.; Scrivens, J. H. *Rapid Commun. Mass Spectrom.* **2008**, *22*, 3297.
(48) Clemmer, D. E.; Jarrold, M. F. *J. Mass Spectrom.* **1997**, *32*, 577.
(49) RCSB Protein Data Bank, http://www.rcsb.org.
(50) Duan, Y.; Chowdhury, S.; Xiong, G.; Wu, C.; Zhang, W.; Lee, T.; Cieplak, P.; Caldwell, J.; Luo, R.; Wang, J.; Kollman, P. A. *J. Comput. Chem.* **2003**, *24*, 1999.
(51) Case, D. A.; Darden, T. A.; Cheatham, T. E., III; Simmerling, C. L.; Wang, J.; Duke, R. E.; Luo, R.; Merz, K. M.; Wang, B.; Pearlman, D. A.; Crowley, M.; Brozell, S.; Tsui, V.; Gohlke, H.; Mongan, J.; Hornak, V.; Cui, G.; Beroza, P.; Schafmeister, C.; Caldwell, J. W.; Ross, W. S.; Kollman, P. A. *Amber03*; University of California, San Francisco, 2004.
(52) Ryckaert, J.-P.; Ciccotti, G.; Berendsen, H. J. C. *J. Comput. Phys.* **1977**, *23*, 327.
(53) Lee, B.; Richards, F. M. *J. Mol. Biol.* **1971**, *55*, 379.
(54) Edelsbrunner, H. *Discrete Comput. Geom.* **1995**, *13*, 415.
(55) Sanner, M.; Olson, A. J.; Spehner, J. C. *Biopolymers* **1996**, *38*, 305.
(56) Wilson, J. A.; Bender, A.; Kaya, T.; Clemons, P. A. *J. Chem. Inf. Model.* **2009**, *49*, 2231.
(57) Garland, M.; Heckbert, P. S. *Proc. Visualization '98* **1998**, 263.
(58) Barber, C. B.; Dobkin, D. P.; Huhdanpaa, H. *ACM Trans. Mathematical Software* **1996**, *22*, 469.
(59) Mason, E. A.; McDaniel, E. W. *Transport properties of ions in gases*; Wiley: New York, 1988.
(60) Kaltashov, I. A.; Mohimen, A. *Anal. Chem.* **2005**, *77*, 5370.
(61) Murphy, P. M.; Baggiolini, M.; Charo, I. F.; Hebert, C. A.; Horuk, R.; Matsushima, K.; Miller, L. H.; Oppenheim, J. J.; Power, C. A. *Pharmacol. Rev.* **2000**, *52*, 145.
(62) Bizzarri, C.; Beccari, A. R.; Bertini, R.; Cavicchia, M. R.; Giorgini, S.; Allegretti, M. *Pharmacol. Ther.* **2006**, *112*, 139.
(63) Clore, G. M.; Appella, E.; Yamada, M.; Matsushima, K.; Gronenborn, A. M. *Biochemistry* **1990**, *29*, 1689.
(64) Spillmann, D.; Witt, D.; Lindahl, U. *J. Biol. Chem.* **1998**, *273*, 15487.
(65) Handel, T. M.; Domaille, P. J. *Biochemistry* **1996**, *35*, 6569.
(66) Lortat-Jacob, H.; Grosdidier, A.; Imberty, A. *Proc. Natl. Acad. Sci. U.S.A.* **2002**, *99*, 1229.
(67) Krieger, E.; Geretti, E.; Brandner, B.; Goger, B.; Wells, T. N.; Kungl, A. J. *Proteins* **2004**, *54*, 768.
(68) Kuschert, G. S.; Hoogewerf, A. J.; Proudfoot, A. E.; Chung, C. W.; Cooke, R. M.; Hubbard, R. E.; Wells, T. N.; Sanderson, P. N. *Biochemistry* **1998**, *37*, 11193.
(69) Ludwig, R. J. *Curr. Drug Discov. Technol.* **2009**, *6*, 281.
(70) Yu, Y.; Sweeney, M. D.; Saad, O. M.; Crown, S. E.; Hsu, A. R.; Handel, T. M.; Leary, J. A. *J. Biol. Chem.* **2005**, *280*, 32200.
(71) Nesmelova, I. V.; Sham, Y.; Gao, J. L.; Mayo, K. H. *J. Biol. Chem.* **2008**, *283*, 24155.